Contrib Mineral Petrol (2010) 159:781–790
DOI 10.1007/s00410-009-0454-x

ORIGINAL PAPER

# The effect of chrysotile nanotubes on the serpentine-fluid Li-isotopic fractionation

**Bernd Wunder · Fabien Deschamps · Anke Watenphul · Stéphane Guillot · Anette Meixner · Rolf L. Romer · Richard Wirth**

Received: 16 July 2009 / Accepted: 6 October 2009 / Published online: 23 October 2009


**Abstract** We determined the lithium isotope fractionation between synthetic Li-bearing serpentine phases lizardite, chrysotile, antigorite, and aqueous fluid in the *P*,*T* range 0.2–4.0 GPa, 200–500°C. For experiments in the systems lizardite-fluid and antigorite-fluid, $^{7}$Li preferentially partitioned into the fluid and $\Delta^{7}$Li values followed the *T*-dependent fractionation of Li-bearing mica-fluid (Wunder et al. 2007). By contrast, for chrysotile-fluid experiments, $^{7}$Li weakly partitioned into chrysotile. This contrasting behavior might be due to different Li environments in the three serpentine varieties: in lizardite and antigorite lithium is sixfold coordinated, whereas in chrysotile lithium is incorporated in two ways, octahedrally and as Li-bearing water cluster filling the nanotube cores. Low-temperature IR spectroscopic measurements of chrysotile showed significant amounts of water, whose freezing point was suppressed due to the Li contents and the confined geometry of the fluid within the tubes. The small inverse Li-isotopic fractionation for chrysotile-fluid results from intra-crystalline Li isotope fractionation of octahedral $Li^{[6]}$ with preference to $^{6}$Li and lithium within the channels ($Li^{[Ch]}$) of chrysotile, favoring $^{7}$Li. The nanotubes of chrysotile possibly serve as important carrier of Li and perhaps also of other fluid-mobile elements in serpentinized oceanic crust. This might explain higher Li abundances for low-*T* chrysotile-bearing serpentinites relative to high-*T* serpentinites. Isotopically heavy Li-bearing fluids of chrysotile nanotubes could be released at relatively shallow depths during subduction, prior to complete chrysotile reactions to form antigorite. During further subduction, fluids produced during breakdown of serpentine phases will be depleted in $^{7}$Li. This behavior might explain some of the Li-isotopic heterogeneities observed for serpentinized peridotites.

**Keywords** Li isotopes · Isotope fractionation · Serpentine phases · Lizardite · Chrysotile · Nanotubes · Antigorite · Subduction zone

Communicated by J. Hoefs.

B. Wunder (✉) · A. Watenphul · A. Meixner · R. L. Romer · R. Wirth
German Research Centre for Geosciences GFZ Potsdam, Telegrafenberg, 14473 Potsdam, Germany
e-mail: wunder@gfz-potsdam.de

F. Deschamps · S. Guillot
Laboratoire de Géodynamique des Chaînes Alpines, CNRS, Université Grenoble I, 1381 rue de la Piscine, 38041 Grenoble Cedex 09, France

## Introduction

Serpentinites are the main product of hydrothermal seawater alteration of ultramafic rocks, notably at slow and ultra-slow spreading ridges. Subduction of serpentinized oceanic lithosphere provides an important mechanism by which water is introduced into the deep mantle (Ulmer and Trommsdorff 1995; Wunder and Schreyer 1997). As serpentinites contain significant amounts of fluid-mobile elements such as B, Cl, Li, As, Sb, these rocks are also likely important for controlling the budgets of these elements in subduction zones (Tenthorey and Hermann 2004; Barnes et al. 2008; Scambelluri et al. 2004; Agranier et al. 2007; Hattori and Guillot 2007).

The three different serpentine varieties lizardite, chrysotile, and antigorite form different structures as response to the misfit of their 1:1 layers composed of octahedral $[Mg_3O_2(OH)_4]^{2-}$ and tetrahedral $[Si_2O_5]^{2-}$

sheets. Lizardite has a flat-layered structure and the misfit is accommodated due to incorporation of smaller ions, e.g., $Li^{+}$ and $Al^{3+}$ for $Mg^{[6]}$, or larger ions, e.g., $Al^{3+}$ and $Fe^{3+}$ for $Si^{[4]}$. The chrysotile structure is roll-layered and forms open tubes, where the tetrahedral component is on the inside of the rolled-up sheet. In the pure system $MgO–SiO_2–H_2O$ (MSH), the chemical composition of these two polymorphs is $Mg_3Si_2O_5(OH)_4$. To minimize the structural misfit, antigorite forms wave-like structures with pressure- and temperature-dependent variation in the a-periodicity, and thus a range of slightly different chemical compositions (Wunder et al. 2001). Compositional variations of antigorite can be expressed by the formula $M_{3m-3}T_{2m}O_{5m}(OH)_{4m-6}$, with M = octahedral cations Mg, Al, and Li, T = tetrahedral cations Si, Al, and B, and $m$ = number of tetrahedra in a single chain along the wavelength $a$ (Kunze 1961).

The stabilities of lizardite and chrysotile in the system $MgO–Al_2O_3–SiO_2–H_2O$ are not well constrained due to sluggish reaction kinetics among serpentine minerals. Both polymorphs can be present concomitantly and form at subseafloor environments down to depths corresponding to temperatures up to 400°C (Mével 2003). During ongoing subduction of serpentinized oceanic lithosphere, lizardite and chrysotile transform to the high-pressure variety antigorite (Evans et al. 1976). Above 660°C (the temperature mainly depends on the Al content of the serpentine phase), antigorite breaks down to chlorite, clinopyroxene, and olivine (Bromiley and Pawley 2003). This reaction produces large amounts of fluid, which trigger formation of melts, metasomatic processes, and seismicity in the overlying mantle wedge (Yamasaki and Seno 2003; Hattori and Guillot 2003; Rüpke et al. 2004).

Lizardite- and chrysotile-bearing serpentinites formed during oceanic floor serpentinization contain small but significant amounts of lithium up to maximum values of 27 ppm (Decitre et al. 2002; Benton et al. 2004; Agranier et al. 2007). Li contents from high-$P$ antigorite-bearing serpentinites of up to 17 ppm (Scambelluri et al. 2004; Deschamps et al. 2009) suggest an abundance lower than in low-$P$ and low-$T$ serpentinites. Serpentinized oceanic peridotites have a remarkably, not well constrained, inhomogeneous Li-isotopic composition, with $\delta^7$Li between −19 and +28‰ (Decitre et al. 2002; Benton et al. 2004). To our knowledge, no systematic investigations of Li isotopes from high-pressure antigorite-bearing serpentinites have been carried out so far.

Strong fractionation of lithium isotopes during geological processes leading to natural variations larger than 60‰ (Tomascak 2004) stem from the large mass difference of about 17% between the two stable Li isotopes $^6$Li and $^7$Li. In conjunction with the establishment of methods for precise Li isotope determination in the last few years, the isotopic composition of lithium in fluids and Li-bearing minerals has been increasingly used to study global-scale processes. However, applying Li isotopes as powerful geochemical tracers, for example to unravel mass transfer processes in subduction zone environments, requires profound knowledge on $T$-dependent equilibrium Li isotope fractionation among Li-bearing minerals and fluids.

Here, we present first experimentally determined Li isotope fractionation data between lizardite, chrysotile, antigorite, and aqueous fluid at 200–500°C and 0.2–4.0 GPa. We will show that significant differences in solid–fluid Li fractionation exist between chrysotile and the two other modifications as a result of varying Li environments.

## Experimental and analytical methods

### Experimental

Serpentine phases generally incorporate lithium as trace element. Experimental data concerning Li incorporation into serpentine are missing. This makes it difficult to design experiments for producing reliable data on Li isotope fractionation. Generally, such experiments need a sufficient Li reservoir in the fluid, so that the forming crystals are isotopically unzoned. This has been recently demonstrated for boron and its isotopes in B isotope fractionation experiments among tourmaline and fluid (Meyer et al. 2008; Marschall et al. 2009). On the other hand, Li concentrations in the fluid at given $P$ and $T$ of the experiment are chosen such that lithium remains in the fluid during quenching and no other solid phase with significant quantities of lithium is formed besides serpentine.

Lithium isotope fractionation between serpentine phases and fluid was determined by crystallizing mixtures of $Li_2O$, $\gamma$-$Al_2O_3$, synthetic brucite, ($Mg(OH)_2$), either synthetic talc ($Mg_3Si_4O_{10}(OH)_2$) in #9, #10 and #22 or $SiO_2$ in #21c, #21d (Table 1) in the presence of excess water. Prior to the Li isotope fractionation experiments, talc was synthesized as single-phase material at 3.0 GPa, 700°C after 48 h from a gel of $3MgO{\cdot}4SiO_2$ composition plus 20 wt.% of excess water, and brucite was synthesized at 0.4 GPa, 600°C, 24 h from MgO plus 30 wt.% of excess water. In latter experiment, about 5 wt.% of periclase (MgO) besides brucite was detected by X-ray powder diffraction. To incorporate Li into serpentine, we chose the coupled substitution mechanism $Li^{[6]} + Al^{[6]} \Leftrightarrow 2Mg^{[6]}$. For the high-pressure experiment #9, aimed to synthesize Li-bearing antigorite, the solid starting materials were mixed in the stoichiometric composition of $[(Mg_{44}Li_2Al_2)Si_{34}]O_{85}(OH)_{62}$ with 0.5 mole% $Li_2O$ in excess. This antigorite composition corresponds to $m$ value of 17, which is the relevant composition for MSH–antigorite at 4.0 GPa, 500°C (Wunder

**Table 1** Summary of experiments and results of ICP MS analyses

| Run # | $P$ (GPa) | $T$ (°C) | $t$ (days) | Solid products | Li in fluid[a] (μmol/l) | Li in solid (ppm) | Li atoms[b] (p.f.u.) | $^{Li}D_{fl/s}$ | Isotopic composition of products (‰) | | |
|---|---|---|---|---|---|---|---|---|---|---|---|
| | | | | | | | | | $\delta^7Li_{solid}$ | $\delta^7Li_{fluid}$ | $\Delta^7Li_{solid-fluid}$ |
| 9 | 4.0 | 500 | 22 | Ant, Chr(tr), Fo(tr) | 3.38 | 360 | 0.23 | 65 | +14.1 | +15.2 | −1.1 |
| 10 | 0.4 | 400 | 14 | Chr, Liz(tr), Fo(tr) | 4.86 | 980 | 0.61[c] | 34 | +15.8 | +14.9 | +0.9 |
| 21d | 0.2 | 200 | 31 | Liz, Chr(tr), Fo(tr) | 5.23 | 440 | 0.27 | 83 | +11.2 | +15.3 | −4.1 |
| 21c | 0.4 | 300 | 31 | Liz, Chr(tr) | 4.80 | 220 | 0.14 | 152 | +13.4 | +16.2 | −2.8 |
| 22 | 0.4 | 400 | 30 | Chr, Liz(tr), Fo(tr) | 4.18 | 1,820 | 1.14[c] | 16 | +15.1 | +14.5 | +0.6 |

Forsterite was identified by XRD, different serpentine varieties by TEM. $1\sigma$ uncertainty in $\delta^7Li_{solid,fluid}$ and $\Delta^7Li_{solid-fluid}$ is 0.5 and 0.7‰, respectively. Assumed errors are larger than 10% for Li concentrations and $^{Li}D_{fl/s}$ values

*Chr* chrysotile, *Liz* lizardite, *Fo* forsterite, *Ant* antigorite, *tr* traces, *fl* fluid, *s* solid, *p.f.u.* per formula unit of serpentine composition of the dominant serpentine phase

[a] Normalized to the amount of solution and of fluid produced during the experiments

[b] Calculated Li contents of serpentine phases refer to structural formulae with 48 octahedral cations and under the assumption that all measured Li is incorporated structurally in octahedral coordination. However, for chrysotile-bearing samples (c), Li is partly incorporated as Li–water cluster filling the nanotubes (for further details, see text)

et al. 2001). Solid starting materials of all low-pressure experiments were mixed in the stoichiometric composition of $[(Mg_{44}Li_2Al_2)Si_{32}]O_{80}(OH)_{64}$ except of #10 and #22, which had 0.5 mole% $Li_2O$ in excess.

For high-pressure synthesis of Li-bearing antigorite at 4.0 GPa, 500°C and 22 days (Table 1), about 20 mg of solid starting material and additional 10 wt.% of water were sealed in an Au capsule of 10 mm × 3 mm with a wall thickness of 0.25 mm. The experiment was performed using an end-loaded piston-cylinder apparatus with NaCl cell, pyrophyllite as pressure medium, and a steel furnace. The estimated pressure accuracy is about ±40 MPa. Temperature was recorded with an accuracy of ±10°C using a Ni–CrNi thermocouple placed closely to the capsule. The sample was quenched to 200°C in less than 15 s. For synthesis of Li-bearing chrysotile and lizardite, about 40–60 mg of the solid starting mixtures and additional 10 wt.% of water were sealed in Au capsules of 25 mm × 5 mm with a wall thickness of 0.5 mm. The experiments were performed at 0.2–0.4 GPa, 200–400°C for 14–31 days (Table 1) using standard cold-seal hydrothermal vessels. The temperature was controlled by Ni–CrNi thermocouples next to the sample position with an accuracy of ±5°C. The pressure was measured with a calibrated strain gauge within an accuracy of ±5 MPa. The experiments were quenched by cooling the autoclaves with compressed air to 100°C in less than 5 min.

After the experiments, the capsules were cleaned, checked for leakage by weighting, and opened by piercing in 80°C hot doubly distilled water to give a total amount of 100 ml for #9, #10 and #22, and 20 ml for #21c and #21d. Solid products were separated from the fluids by filtration. Small possible amounts of solid nano-particles dispersed in the diluted fluid were extracted with an ultracentrifuge at 50,000 turns/min for a few hours. Bulk fluid and centrifuged effluent were carefully separated from each other and both were analyzed for their Li isotope composition. Differences in $\delta^7Li$ were always smaller than ±0.2‰ indicating no significant nano-particles dispersion within the fluids.

## Analytical

### *Powder X-ray diffraction (XRD)*

Solid run products were characterized by powder XRD using a Stoe Stadi P diffractometer in the 2Θ range from 5° to 125° for CuK$\alpha_1$ radiation.

### *Transmission electron microscopy (TEM)*

Specific foils of about 0.2 μm thickness were cut from epoxy-embedded samples using a Fei FIB200 focused ion beam devise with Ga-ion source. Details of the application of the FIB technique are given in Wirth (2004). The foils were placed onto carbon grids for TEM analyses. Identification and characterization of the different serpentine types were performed with TEM Fei Tecnai $G^2$ F20 X-Twin at 200 kV, equipped with a FEG electron source, a Fischione high angle annular field detector (HAADF), and a Gatan imaging filter (Tridiem) for acquisition of energy-filtered images. EDX analyses were performed by scanning the electron beam in a window of approximately 100 nm × 100 nm.

### *Infrared (IR) spectroscopy*

Infrared spectroscopic measurements at room temperature were carried out on KBr pellets. 1 mg of the run products

was ground and dispersed into 450 mg KBr. The homogenized mixture was cold-pressed under vacuum into 13 mm diameter pellets and dried for 2 days at 170°C.

The IR spectra were collected with a Bruker IFS 66v FTIR spectrometer equipped with a KBr beam splitter, a Globar light source, and a DTGS detector in the spectral region 4,000–400 $cm^{-1}$ with a resolution of 2 $cm^{-1}$. Spectra were averaged over 256 scans.

Low-*T* IR measurements were carried out on thin sample films of about 7 μm thickness. Ground sample material was dried for 2 days at 100°C to avoid fluid loss from the chrysotile nanotube cores (see below). Thin film preparation is described in detail in Watenphul and Wunder (2009). IR spectra were collected using a Hyperion microscope with a MCT detector attached to the Bruker spectrometer. The sample film was mounted on a glass carrier and placed into a Linkam FTIR600 heating/cooling stage of the microscope. Spectra were recorded between +20 and −100°C in the spectral region 4,000–3,000 $cm^{-1}$ with a resolution of 1 $cm^{-1}$ and averaged over 512 scans.

After linear background correction, band positions, full widths at half maximum (FWHM) and integrated intensities were determined using the program PeakFit by Jandel Scientific. The autocorrelation method (Salje et al. 2000) was applied to the low-*T* IR spectra in the spectral range 3,500–3,000 $cm^{-1}$ to obtain the water–ice transformation temperature. The content $c$ of molecular water in the chrysotile tubes was calculated from the integrated intensities $A_i$ of the water bands in the 20°C spectrum using the equation: $c$ (wt.% $H_2O$) = $A_i$ ($cm^{-1}$) × 1.8/[$t$ (cm) × $D$ (g/$cm^3$) × 3$\varepsilon_i$ ($cm^{-2}$ per mol $H_2O$/l)], with $t$ = sample thickness, $D$ = density of chrysotile, $\varepsilon_i$ = integrated molar absorption coefficient (Libowitzky and Rossman 1997).

### Multi-collector-inductively coupled plasma mass spectroscopy (MC-ICP MS)

Lithium concentration and Li-isotopic composition of solid and fluid run products were determined using a MC-ICP MS Neptune Thermofisher Scientific. Sample preparation, international rock standard, and seawater analyzed during this study to control the analytical procedure, operating conditions, and measurement procedure are nearly identical to those reported by Wunder et al. (2006) combined with the slight modifications described by Wunder et al. (2007). Isotopic analyses are given as per mil variations in the lithium composition of a sample relative to the lithium isotope standard NIST 8545, according to $\delta^7Li = \{[(^7Li/^6Li)_{sample}/(^7Li/^6Li)_{standard}] - 1\} \times 1{,}000$. During this study, repeatedly measured through the whole chemistry, NIST 8545 shows a $\delta^7Li$ of $-0.1 \pm 0.4$‰ ($2\sigma$, $n = 3$). The $1\sigma$ uncertainty in $\delta^7Li_{solid,fluid}$ is <0.5‰; the Li isotope fractionation is defined as $\Delta^7Li_{solid-fluid} = \delta^7Li_{solid} - \delta^7Li_{fluid}$. The starting material $Li_2O$ had the Li-isotopic composition $\delta^7Li = +14.8 \pm 0.5$‰. Due to the presence of small Au flakes from the sample containers, the determined Li contents of solids are rather inaccurate and represent minimum values. For Li contents and calculated fluid/solid Li partition coefficients $^{Li}D_{fl/s}$, we estimate errors larger than 10%.

## Results

### Description of run products

#### *X-ray diffraction*

As characterized by XRD, all experiments produced serpentine phases as the dominant solid phase along with traces of forsterite in runs #9, #10, #21d and #22 (Table 1). All serpentine reflections are very broad, indicating very small crystal sizes of the run products. The width of reflections hindered an unambiguous identification of the serpentine variety.

#### *TEM*

The morphology of serpentine phase formed during the experiments was characterized by TEM. We refer to the type of serpentine phase as later verified by IR (see below). No quench phase was detected. In the high-pressure experiment #9, mainly thin flakes of antigorite are visible (Fig. 1a) together with minor amounts of chrysotile tubes. Both experiments #10 (Fig. 1b) and #22, performed at 0.4 GPa and 400°C, yielded chrysotile tubes as major serpentine phase together with small amounts of thin lizardite flakes. In the experiments performed at low temperatures of 300°C at 0.4 GPa (#21c) and 200°C at 0.2 GPa (#21d), very small and thin flakes of lizardite were synthesized together with traces of chrysotile in #21c (Fig. 1c) and minor amounts of chrysotile in #21d (Fig. 1d). In all experiments, crystals of serpentine phases have nanometer dimensions, ranging from a few hundred nanometers for antigorite formed at 500°C (#9) to only a few nanometers for lizardite formed at 200°C (#21d). Chrysotile tubes have inner core diameters of 4–7 nm. The outer diameters of 15 and 35 nm are consistent with the presence of single- and double-tube structures (Foresti et al. 2005).

As determined from EDX analyses, Al contents do not vary significantly between serpentine phases from the different runs. The concentrations range between 1.3 and 2.7 wt.% $Al_2O_3$, which correspond to about 1–2 Al per formula unit (based on 48 octahedral cations). Taking into account the Li contents from ICP MS measurements (see

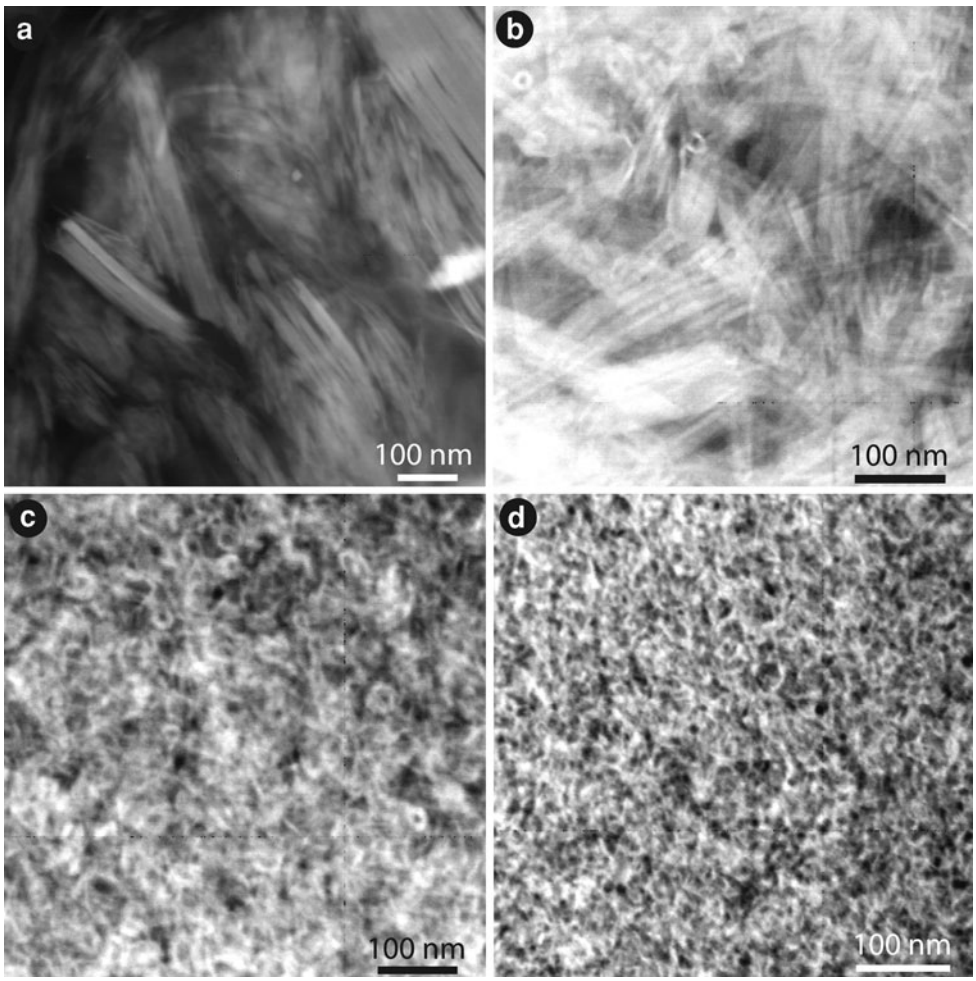


**Fig. 1** TEM (HAADF) images of **a** antigorite (#9, Table 1), **b** chrysotile (#10), **c** lizardite with traces of chrysotile (#21c) and **d** lizardite (#21d)

below, Table 1), the high Al contents might indicate that besides the assumed $^{[6]}Li_1^{[6]}Al_1^{[6]}Mg_{-2}$ substitution, Al is also incorporated into the serpentine phases according to Tschermak's substitution.

In summary, the dominant serpentine phases formed in the experiments are lizardite at low pressures, 0.2–0.4 GPa, and low temperatures, 200–300°C, chrysotile at 0.4 GPa and 400°C, and antigorite at higher pressure, 4.0 GPa, and 500°C.

*IR spectroscopy*

In Fig. 2, room temperature IR spectra of the samples #9, #10, and #21c are shown, which exhibit predominantly the serpentine varieties antigorite, chrysotile, and lizardite, respectively. The main OH band, which is attributed to hydroxyl neighboring $Mg^{[6]}$ (outer OH band after Velde 1980), occurs for antigorite (3,689 $cm^{-1}$) at lower wavenumbers than for chrysotile (3,695 $cm^{-1}$) and lizardite (3,696 $cm^{-1}$). This is in accordance with Lemaire et al. (1999) and Auzende et al. (2004), who showed that the outer OH band of antigorite has the lowest frequency of the three serpentine types. Further OH bands in the range of the OH stretching vibrations can partly be attributed to hydroxyls, for which the neighboring octahedral sites are filled with ions different than $Mg^{2+}$ (Velde 1980). These OH bands occur in each of the three spectra shown in Fig. 2, indicating $Mg^{[6]}$ exchange according to substitution vectors $^{[6]}Li_1^{[6]}Al_1^{[6]}Mg_{-2}$ and $^{[4]}Al_1^{[6]}Al_1^{[4]}Si_{-1}^{[6]}Mg_{-1}$. The basic Si–O stretching frequencies of serpentine phases appear in the spectral range 1,100–900 $cm^{-1}$. Without any tetrahedral Al substitution for Si, generally three bands should occur for each serpentine type (Velde 1980; Balan et al. 2002). The antigorite and lizardite spectra in Fig. 2 display only two bands, whereas in the chrysotile spectrum three bands are distinguishable. However, this is in agreement with Velde (1980) and Balan et al. (2002), who describe an overlap of the two low-energy bands of antigorite and lizardite.

IR spectra at 20 and −100°C of the thin film of the mainly chrysotile-bearing sample #10 are shown in Fig. 3. Broad OH bands are visible in the spectral region 3,500–3,000 $cm^{-1}$, which were not observed for lizardite- and antigorite-bearing samples. These bands are associated

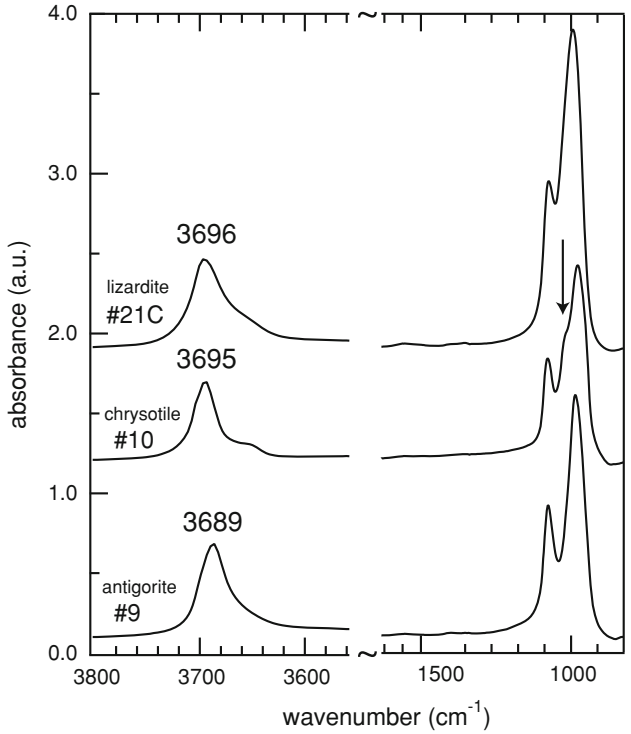


**Fig. 2** Room temperature IR spectra of #9 (antigorite), #10 (chrysotile), and #21c (lizardite). Spectra are offset for clarity. *Arrow* indicates typical band splitting for chrysotile in the frequence range of Si–O stretching vibrations (see text for further information)

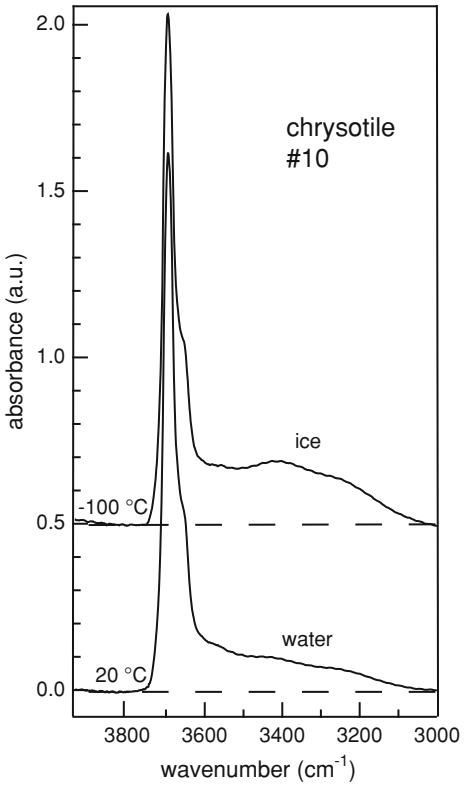


**Fig. 3** IR spectra of pure chrysotile (#10) showing the transformation of molecular water in the nanotubes at 20°C to ice at −100°C

with molecular water at 20°C and with ice at −100°C. The water content of this sample was calculated from the integrated intensities at 20°C to about 1,800 ppm $H_2O$.

We measured IR spectra of sample #10 at various low temperatures between 20 and −50°C. The autocorrelation method (Salje et al. 2000) was applied on the taken low-temperature spectra to obtain effective linewidth of the complex overlapping band structure. The discontinuity in the changing behavior of the linewidths, expressed as ΔCorr in Fig. 4, indicates the phase transition from water to ice at about −39°C. This strong suppression of the freezing point of ice reveals the effect of dissolved Li in the fluid combined with the confined geometry of the Li–water clusters within the tubes, and absence of absorbed water.

## Li contents measured by MC-ICP MS

Li values of solids determined by MC-ICP MS can solely be assigned to the individual serpentine phases because forsterite is only present as minor amount in four experiments and has low Li concentrations. We determined Li contents ranging from 220 to 1,820 ppm (Table 1) for the five solid samples. The highest amounts of Li were determined for the two experiments mainly containing chrysotile (#10, #22).

In all experiments, lithium preferentially partitioned into the fluid over the serpentine phases. Fluid/solid Li partition

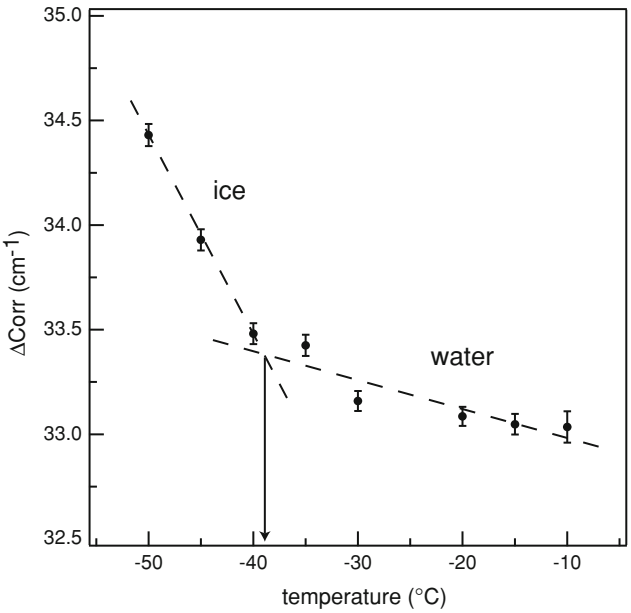


**Fig. 4** Variation of ΔCorr with temperature obtained from autocorrelation analysis of the IR spectra in the frequency range 3,500–3,000 $cm^{-1}$. *Dashed lines* are derived from linear fits of the data points. Intersection of *dashed lines* indicates the suppressed transition temperature from water to ice (for more details, see text); *arrow* points to the relevant temperature

coefficient $^{Li}D_{fl/s}$ (Table 1) ranges from 16 for run #22 in which chrysotile formed as the main serpentine phase to 152 for the lizardite-bearing run #21c. Literature data of $^{Li}D_{fl/s}$ values for serpentine fluid from experiments are lacking. Tenthorey and Hermann (2004) determined $^{Li}D_{fl/s}$ values of 100 for residual phases and fluids from antigorite breakdown at 3.0 GPa and 750°C.

Assuming that all measured Li is incorporated octahedrally according to the $^{[6]}Li_{1}^{[6]}Al_{1}^{[6]}Mg_{-2}$ substitution and calculating the structural formulae for serpentine phases as given before for the stoichiometric compositions of the starting materials on the basis of 48 octahedral cations yielded 0.14–1.14 Li atoms per formula unit (Table 1). However, as we will show below, these values do not apply for samples with chrysotile as main serpentine phase (#10, #22), because some of the Li form Li–water clusters in the channels of chrysotile.

### Fractionation of Li isotopes between serpentine varieties and fluid

The results of lithium isotopic fractionation of all experiments are summarized in Table 1 and in Fig. 5. Due to small amounts of forsterite in some of the samples and its generally minute Li contents, measured Li isotope fractionation between bulk solids and fluids is not significantly affected by the presence of forsterite. Because of the much higher Li concentration in the fluid than in coexisting solids, $\delta^7Li_{fluid}$ values are near the isotopic composition of the starting material, except for #21c (Table 1), which has an unusually high $\delta^7Li_{fluid}$ value. The difference to the isotopic composition of the starting material is within $2\sigma$ uncertainty. The other measured $\delta^7Li_{fluid}$, $\delta^7Li_{solid}$ values and serpentine-fluid fractionation data fit within $1\sigma$ uncertainty.

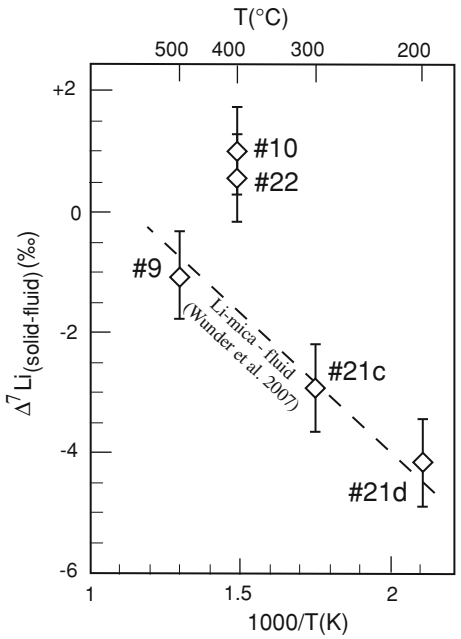


**Fig. 5** Plot of experimentally determined isotopic fractionation of lithium versus reciprocal temperature between serpentine varieties and fluid. For comparison, the Li isotope fractionation for Li–mica-fluid (Wunder et al. 2007) is shown

In experiments with lizardite or antigorite as main serpentine phase, $^7$Li preferentially fractionated into the fluid. As shown in Fig. 5, the corresponding $\Delta^7$Li values follow the *T*-dependent fractionation recently determined for Li–mica-fluid (Wunder et al. 2007). On the contrary, in the two experiments #10 and #22 performed at 0.4 GPa and 400°C, with chrysotile crystallizing as the main serpentine phase, $^7$Li slightly favored the solid. Experimental conditions of these two experiments varied only in run duration. They resulted in nearly identical Li-isotopic fractionation, indicating that isotopic equilibrium had been reached in the experiments.

## Discussion

There is overall agreement that the first-order effect responsible for lithium isotope fractionation between solid and fluid is the change of octahedrally coordinated lithium in most silicates (Wenger and Armbruster 1991), except Li-staurolite (Dutrow 1991), to fourfold clustered $[Li(H_2O)_4]^+$ complexes in aqueous fluids (Yamaji et al. 2001). Furthermore, the lighter isotope should preferentially occupy the higher coordinated site (Schauble 2004). This is in particular the case of our experiments, which were all performed at low temperatures and where Li isotope fractionation is not transport controlled due to differences in diffusivities of light and heavy isotope, which is relevant at high temperatures (e.g., Richter et al. 2003; Lundstrom et al. 2005). The pressures of our experiments are not high enough to form significant amounts of Li–water cluster in the fluid that are higher coordinated than $[Li(H_2O)_4]^+$, which would affect the extent of Li isotope fractionation (Jahn and Wunder 2009). The good consistency of $\Delta^7$Li values for antigorite-fluid and lizardite-fluid experiments with *T*-dependent $\Delta^7$Li values of Li–mica-fluid (Wunder et al. 2007) indicates that (1) lithium is sixfold coordinated in antigorite and lizardite equally to Li–mica, (2) the bonding environments of Li are similar for all the three phyllosilicates, and (3) the small grain sizes of serpentine phases do not significantly affect the Li isotope fractionation. Such grain size-dependent effects on Li isotope fractionation have recently been described between clay minerals and fluids (Williams and Hervig 2005). The inverse fractionation of Li isotopes relative to fluids in runs #10 and #22 indicates that the

coordination of Li in chrysotile is lower than six folded. Due to its single valency and its large ionic radius of 0.76 Å (Shannon 1976), we exclude tetrahedrally coordinated Li in the structure of chrysotile and assume a model, in which some of the lithium is incorporated as Li-bearing water clusters filling the nanotube cores.

Since five decades, it is known that chrysotile tubes can incorporate various kinds of materials, which change the physical and chemical properties of chrysotile (Mellini 2005; and references therein). Bates and Comer (1959) reported amorphous material within chrysotile tubes. Cl-bearing amorphous material has recently been found in natural chrysotile from seafloor serpentinites and is discussed as important carrier of chlorine in subduction zone environments (Brearley et al. 2007). Aimed to study technologic aspects and to tailor electrical properties of chrysotile, Métraux et al. (2002) and Grobéty et al. (2004) incorporated molten Pb and Hg into the tubes. Maslennikova et al. (2008) studied the filling of chrysotile nanochannels by aqueous KOH-bearing solution at various conditions. Takamuku et al. (1997) incorporated pure water into chrysotile tubes and measured suppressed freezing points, which are close to our determined value. Interestingly, they found that the suppression of the freezing point depends on the tube diameter, with a decrease of the freezing point for decreasing diameter (Ø 3 nm: −36°C; Ø 10 nm: −21°C). The water–ice transition of chrysotile from #10 occurs at lower temperatures of −39°C, indicating dissolution of significant amounts of Li in the nanotube fluid, because tube diameter ranges between 4 and 7 nm.

We propose that the inverse Li-isotopic fractionation between chrysotile and fluid is affected by the incorporation of $[Li(H_2O)_4]^+$ clusters into the serpentine nanotubes ($Li^{[Ch]}$). The observed isotopic fractionation is due to differences in the chemical potential for lithium dissolved in the bulk water and $Li^{[Ch]}$ of the Li–water clusters in the confinement of the tubes, which are perturbed by forming bonds to oxygen of the $[SiO_4]^{4-}$ tetrahedra at the inside of the channels. The significant suppression of the freezing point is a clear indicator for the energetic difference in bonding for lithium between Li-bearing bulk and the more rigidly bonded confined water. If the freezing point is a function of the size of the nanotube diameter (Takamuku et al. 1997), this perhaps also holds for the Li-isotopic fractionation: the smaller the tube diameter, the larger the energetic difference of Li in tube fluid compared to bulk fluid, resulting in a stronger Li isotope fractionation. However, more experimental work is needed to confirm these assumptions.

The total amount of Li in chrysotile and the overall $\Delta^7Li_{chrysotile\text{-}fluid}$ result from the sum of individual concentrations of $Li^{[Ch]}$ and $Li^{[6]}$ and from the individual isotopic fractionations $\Delta^7Li^{[Ch]}_{chyrosotile\text{-}fluid}$ and $\Delta^7Li^{[6]}_{chrysotile\text{-}fluid}$, respectively. Under the assumption that the amount of $Li^{[6]}$ in chrysotile is about the same as found for lizardite and antigorite in our experiments, we estimate about 340 ppm $Li^{[6]}$ (mean value of the runs #9, #21d, and #21c). Further expecting the same *T*-dependent Li-isotopic fractionation for $\Delta^7Li^{[6]}_{chrysotile\text{-}fluid}$ as determined for antigorite-fluid, lizardite-fluid (both this study), and Li–mica-fluid (Wunder et al. 2007), $\Delta^7Li^{[6]}_{chrysotile\text{-}fluid}$ is about −1.5‰ at 400°C. If so, calculations of $\Delta^7Li^{[Ch]}_{chrysotile\text{-}fluid}$ and an intra-crystalline Li-isotopic fractionation ($\Delta^7Li^{[6]}_{chrysotile\text{-}fluid} - \Delta^7Li^{[Ch]}_{chrysotile\text{-}fluid}$) result for #10 in +2.2 and −3.7‰, and for #22 in +1.1 and −2.6‰, respectively.

Our data suggest that chrysotile tubes may be an important carrier of Li and perhaps also for other fluid-mobile elements (e.g., B, Cl) in serpentinized oceanic crust. Further, we assume two Li incorporation mechanism for chrysotile—$Li^{[Ch]}$ and $Li^{[6]}$—and an intra-crystalline Li isotope fractionation between $Li^{[Ch]}$ and $Li^{[6]}$. During subduction of chrysotile-bearing serpentinites, fluids from the nanotubes can be released at relatively shallow depths close to the trench position. This is in-line with the observation that low-*T* chrysotile-bearing serpentinites often have highest Li(B,Cl) abundances (e.g., Savov et al. 2005; Vils et al. 2009). Furthermore, near-surface formed serpentinites often have heavy Li-isotopic composition (e.g., Benton et al. 2004; Chan et al. 2006). This is in agreement with our assumption that nanotube dehydration of chrysotile at low temperatures produces fluids enriched in $^7Li$. The dehydration of chrysotile tubes will probably occur prior to the complete dehydration of chrysotile, which would then produce a fluid depleted in $^7Li$. The large range of Li isotope compositions in serpentinized oceanic crust might therefore be explained from combined effects: (1) significantly different Li-isotopic fractionation of chrysotile-fluid in comparison to lizardite-fluid at low temperatures, and (2) stepwise dehydration of chrysotile producing different Li isotope reservoirs. During further subduction and transformation of only $Li^{[6]}$-bearing chrysotile and lizardite into antigorite, the light Li isotope component will be transported to larger depths, until the breakdown of antigorite. Together with Li-isotopic fractionation during progressive dehydration of oceanic lithosphere (Wunder et al. 2006), this would be another mechanism to transport successively lighter Li isotopes into the mantle during subduction. The liberated fluids from decomposed antigorite percolate through the mantle wedge until reaching the site of magma generation. However, due to high Li abundance of mantle minerals (Seitz and Woodland 2000) and diffusive Li redistribution in the sub-arc mantle (Halama et al. 2009), the fluids do not

remain unaltered. As a consequence, arc lavas do not show systematic variations in Li concentration and Li isotopes across the arc (except for the Izu arc; Moriguti and Nakamura 1998).

## Conclusions

Our study reinforces the idea that subduction and subsequent dehydration of serpentinites play a major role in the fluid-mobile element recycling into the upper mantle and fore-arc magma regions (e.g., Hattori and Guillot 2003; Staub and Layne 2002). Intriguing possibilities coming from our data are that the nanotubes of chrysotile serve as important carrier of Li and perhaps also for other fluid-mobile elements in serpentinized oceanic crust. Despite the limited data set, the indication that Li isotope fractionation is strongly influenced by this "special" structural incorporation mechanism is compelling. For now, we can only offer the mentioned possibilities for consideration. Our preliminary data and speculations will require additional testing and we hope that further experiments and investigations on isotopic composition of natural serpentines, considering the different varieties, are encouraged by this study.

**Acknowledgments** The authors are grateful to G. Berger and A. Schreiber for sample preparation and to H.-P. Nabein for technical assistance in the hydrothermal laboratory. Thanks to M. Barth of the Max Planck Institute of Colloids and Interfaces, Potsdam for centrifuging our fluids. This work was supported by PROCOPE programs. We thank I.P. Savov and an anonymous reviewer for their constructive reviews, and W. Heinrich for his critical and constructive comments on an earlier version of the manuscript.

## References

Agranier A, Lee CTA, Li ZXA, Leeman WP (2007) Fluid-mobile element budgets in serpentinized oceanic lithospheric mantle: insights from B, As, Li, Pb, PGEs and Os isotopes in the Feather River Ophiolite, California. Chem Geol 245:230–241

Auzende AL, Daniel I, Reynard B, Lemaire C, Guyot F (2004) High-pressure behaviour of serpentine minerals: a Raman spectroscopic study. Phys Chem Miner 31:269–277

Balan E, Mauri F, Lemaire C, Brouder C, Guyot F, Saitta AM, Devouard B (2002) Multiple ionic-plasmon resonances in naturally occurring multiwall nanotubes: infrared spectra of chrysotile asbestos. Phys Rev Lett 89:177401-1–177401-4

Barnes JD, Sharp ZD, Fischer TP (2008) Chlorine isotope variations across the Izu-Bonin-Mariana arc. Geology 36(11):883–886

Bates TF, Comer JJ (1959) Further observations on the morphology of chrysotile and halloysite. In: Proceedings of the 6th national conference on clay and clay minerals, pp 237–248

Benton LD, Ryan JG, Savov IP (2004) Lithium abundance and isotope systematics of forearc serpentinites, Conical Seamounts, Mariana forearc: insights into the mechanics of slab-mantle exchange during subduction. Geochem Geophys Geosyst 5:8. doi:10.1029/2004GC000708

Brearley AJ, Barnes JD, Sharp ZD (2007) Chrysotile nanotubes: potential host of insoluble chlorine in serpentinized oceanic crust. Abstracts of AGU Fall Meeting, #V11E-04

Bromiley GD, Pawley AR (2003) The stability of antigorite in the systems $MgO–SiO_2–H_2O$ (MSH) and $MgO–Al_2O_3–SiO_2–H_2O$ (MASH): the effect of $Al^{3+}$ substitution on high-pressure stability. Am Mineral 88:99–108

Chan LH, Savov IP, Ryan JG (2006) Lithium isotope study of peridotite-slab fluid interactions in the Mariana mantle wedge. Abstracts of AGU Fall Meeting, #V43A-03

Decitre S, Deloule E, Reisberg L, James R, Agrinier P, Mével C (2002) Behavior of Li and its isotopes during serpentinization of oceanic peridotites. Geochem Geophys Geosyst 3:1. doi:10.1029/2001GC000178

Deschamps F, Guillot S, Godard M, Chauvel C, Andreani M, Hattori K (2009) In situ characterization of serpentinites from forearc mantle wedges: Timing of serpentinization and behaviour of fluid-mobile elements in subduction zones. Chem Geol (in press). doi:10.1016/j.chemgeo.2009.10.002

Dutrow BL (1991) The effects of Al and vacancies on Li substitution in iron staurolite: a synthesis approach. Am Mineral 76:42–48

Evans BW, Johannes W, Oterdoom H, Trommsdorff V (1976) Stability of chrysotile and antigorite in the serpentinite multisystem. Schweizer Mineral Petrogr Mitt 56:79–93

Foresti E, Hochella MF Jr, Kornishi H, Lesci IG, Madden AS, Roveri N, Xu H (2005) Morphological and chemical/physical characterization of Fe-doped synthetic chrysotile nanotubes. Adv Funct Mater 15:1009–1016

Grobéty BH, Métraux C, Ulmer P (2004) Chrysotile, a template for metal nanowires. Abstracts of 32nd International Geological Congress, p 308

Halama R, Savov IP, Rudnick RL, McDonough F (2009) Insights into Li and Li isotope cycling and sub-arc metasomatism from veined mantle xenoliths, Kamchatka. Contrib Mineral Petrol 158:197–222

Hattori KH, Guillot S (2003) Volcanic fronts as consequence of serpentine dehydration in mantle wedge. Geology 31:525–528

Hattori KH, Guillot S (2007) Geochemical character of serpentinites associated with high- to ultrahigh-pressure metamorphic rocks in the Alps, Cuba, and the Himalayas: recycling of elements in subduction zones. Geochem Geophys Geosyst 8:9. doi:10.1029/2007GC001594

Jahn S, Wunder B (2009) Lithium speciation in aqueous fluids at high *P* and *T* studied by ab initio molecular dynamics and consequences for Li-isotope fractionation between minerals and fluids. Geochim Cosmochim Acta 73:5428–5434

Kunze G (1961) Antigorit. Strukturtheoretische Grundlagen und ihre praktische Bedeutung für die weitere Serpentin-Forschung. Fortschr Mineral 39:206–324

Lemaire C, Guyot F, Reynard B (1999) Vibrational spectroscopy (IR and Raman) of OH groups in chrysotile, lizardite and antigorite. European Union of Geosciences 10, Journal of Conference Abstracts 4, p 654

Libowitzky E, Rossman GR (1997) An IR absorption calibration for water in minerals. Am Mineral 82:1111–1115

Lundstrom CC, Chaussidon M, Hsui AT, Keleman P, Zimmerman M (2005) Observations of Li isotopic variations in the trinity ophiolite: evidence for isotopic fractionation by diffusion during mantle melting. Geochim Cosmochim Acta 69:735–751

Marschall HR, Meyer C, Wunder B, Ludwig T, Heinrich W (2009) Experimental boron-isotope fractionation between tourmaline and fluid: confirmation from in situ analyses by secondary-ion mass spectroscopy and from Rayleigh fractionation modeling. Contrib Mineral Petrol 158:675–681

Maslennikova TP, Korytkova EN, Gusarov VV (2008) Interaction of $Mg_3Si_2O_5(OH)_4$ nanotubes with potassium hydroxide. Russ J Appl Chem 81(3):375–379

Mellini M (2005) Micro- and mesoporous carbon forms, chrysotile, and clathrates. In: Ferraris G, Merlino S (eds) Micro- and mesoporous mineral phases. Rev Mineral Geochem 57:435–448

Métraux C, Grobéty BH, Ulmer P (2002) Filling of chrysotile nanotubes with metals. J Mater Res 17:1129–1135

Mével C (2003) Serpentinization of abyssal peridotites at mid-ocean ridges. Comtes Rendus Geosci 335:825–852

Meyer C, Wunder B, Meixner A, Romer RL, Heinrich W (2008) Boron-isotope fractionation between tourmaline and fluid: an experimental re-investigation. Contrib Mineral Petrol 156:259–267

Moriguti T, Nakamura E (1998) Across-arc variation of Li isotopes in lavas and implications for crust/mantle recycling at subduction zones. Earth Planet Sci Lett 163:167–174

Richter FM, Davis AM, DePaolo DJ, Watson B (2003) Isotope fractionation by chemical diffusion between molten basalt and rhyolite. Geochim Cosmochim Acta 67:3905–3923

Rüpke LH, Morgan JP, Hort M, Connolly JAD (2004) Serpentine and the subduction water cycle. Earth Planet Sci Lett 223:17–34

Salje E, Carpenter MA, Malcherek T, Boffa-Ballaran T (2000) Autocorrelation analysis of infrared spectra from minerals. Eur J Mineral 12:503–519

Savov IP, Ryan JG, D'Antonio M, Kelley K, Mattie P (2005) Geochemistry of serpentinized peridotites from the Marina Forearc Conical Seamount, ODP Leg 125: Implications for the elemental recycling at subduction zones. Geochem Geophys Geosyst 6. doi:10.1029/2004GC000777

Scambelluri M, Müntener O, Ottolini L, Pettke TT, Vannucci R (2004) The fate of B, Cl and Li in the subducted oceanic mantle and in the antigorite breakdown fluids. Earth Planet Sci Lett 222:217–234

Schauble EA (2004) Applying stable isotope fractionation theory to new systems: In: Johnson CM, Beard BI, Albarede F (eds) Geochemistry of non-traditional stable isotopes. Rev Mineral Geochem 55:65–111

Seitz H-M, Woodland AB (2000) The distribution of lithium in peridotitic and pyroxenitic mantle lithologies—an indicator of magmatic and metasomatic processes. Chem Geol 166:47–64

Shannon RD (1976) Revised effective ionic radii and systematic studies of interatomic distances in halides and chalcogenides. Acta Crystallogr A 32:751–767

Staub SM, Layne GD (2002) The systematics of boron isotopes in Izu arc front volcanic rocks. Earth Planet Sci Lett 198:25–39

Takamuku T, Yamagami M, Wakita H, Masuda Y, Yamaguchi T (1997) Thermal property, structure, and dynamics of supercooled water in porous silica by calorimetry, neutron scattering, and NMR relaxation. J Phys Chem B 101:5730–5739

Tenthorey E, Hermann J (2004) Compositions of fluids during serpentinite breakdown in subduction zones: evidence for limited boron mobility. Geology 32(10):865–868

Tomascak PB (2004) Developments in the understanding and application of lithium isotopes in the earth and planetary sciences. In: Johnson CM, Beard BI, Albarede F (eds) Geochemistry of non-traditional stable isotopes. Rev Mineral Geochem 55:153–195

Ulmer P, Trommsdorff V (1995) Serpentine stability to mantle depths and subduction related magmatism. Science 268:858–861

Velde B (1980) Ordering of synthetic aluminous serpentinites; infrared spectra and cell dimensions. Phys Chem Miner 6:209–220

Vils F, Kalt A, Müntener O, Ludwig T (2009) Light elements in oceanic and ophiolitic serpentinites and implications for element recycling in subduction zones. Geochim Cosmochim Acta Suppl 73:A1386

Watenphul A, Wunder B (2009) Temperature dependence of the OH-stretching frequencies in topaz-OH. Phys Chem Miner (in press). doi:10.1007/s00269-009-0310-6

Wenger M, Armbruster T (1991) Crystal chemistry of lithium: oxygen coordination and bonding. Eur J Mineral 3:387–399

Williams LB, Hervig RL (2005) Lithium and boron isotopes in illite–smectite: the importance of crystal size. Geochim Cosmochim Acta 69:5705–5716

Wirth R (2004) Focused ion beam (FIB): a novel technology for advanced application of micro- and nanoanalysis in geosciences and applied mineralogy. Eur J Mineral 16:863–876

Wunder B, Schreyer W (1997) Antigorite: high-pressure stability in the system $MgO–SiO_2–H_2O$ (MSH). Lithos 41:213–227

Wunder B, Wirth R, Gottschalk M (2001) Antigorite: pressure and temperature dependence of polysomatism and water content. Eur J Mineral 13:485–495

Wunder B, Meixner A, Romer RL, Heinrich W (2006) *T*-dependent isotopic fractionation of lithium between clinopyroxene and high-pressure hydrous fluids. Contrib Mineral Petrol 151:112–120

Wunder B, Meixner A, Romer RL, Feenstra A, Schettler G, Heinrich W (2007) Lithium isotope fractionation between Li-bearing staurolite, Li–mica and aqueous fluids: an experimental study. Chem Geol 238:277–290

Yamaji K, Makita Y, Watanabe H, Sonoda A, Kanoh H, Hirotsu T, Ooi K (2001) Theoretical estimation of lithium isotopic reduced partition function ratio of lithium ions in aqueous solution. J Phys Chem A 105:602–613

Yamasaki T, Seno T (2003) Double seismic zone and dehydration embrittlement of the subducting slab. J Geophys Res 108:B4. doi:10.1029/2002JB001918